### Proceedings 10th NUMGE 2023

10th European Conference on Numerical Methods in Geotechnical Engineering Zdravković L, Konte S, Taborda DMG, Tsiampousi A (eds)

ISSN

© Authors: All rights reserved, 2023 doi: 10numge-2023-Y-XXXX

# Numerical analyses of a multiline ring anchor for floating offshore wind turbines in sand

Ragini Gogoi<sup>1</sup>, Anas S. Aldawwas<sup>2</sup>, Charles P. Aubeny<sup>1</sup>, Alejandro Martinez<sup>3</sup>, Lin Huang<sup>3</sup>, Don J. DeGroot<sup>4</sup>, Sanjay R. Arwade<sup>4</sup>, Ryan Beemer<sup>5</sup>

<sup>1</sup>Department of Civil Engineering, Texas A&M University, College Station, USA

<sup>2</sup>Department of Civil Engineering, Qassim University, Unaizah, Saudi Arabia

<sup>3</sup>Department of Civil Engineering, University of California, Davis, USA

<sup>4</sup>Department of Civil Engineering, University of Massachusetts, Amherst, USA

<sup>5</sup>Department of Civil Engineering, University of Massachusetts, Dartmouth, USA

**ABSTRACT:** The multiline ring anchor (MRA) is a novel anchor system proposed for the emerging floating offshore wind technology. The ring-shaped anchor concept comprises of an embedded ring anchor connected to multiple mooring lines, allowing sharing of anchors amongst multiple platforms, and thus resulting in a significant reduction of the total number of anchors and installations required. Apart from being cost efficient, the MRA can be installed deep into the seabed, resulting in the mobilisation of a higher soil resistance. The present paper assesses the performance of the MRA in sand soils where its behaviour is investigated under monotonic loading conditions using a three-dimensional (3D) finite element (FE) model capable of making reliable estimates of axial and lateral ultimate capacities. Data on the anchor's behaviour from centrifuge tests under similar loading conditions are employed as a calibrating tool for the numerical model.

Keywords: Multi-line anchor, floating offshore wind farm

#### 1 INTRODUCTION

A significant step in the progress of the offshore wind energy sector has been the introduction of the floating offshore wind turbine (FOWT) concept. Motivated by the abundance of offshore wind resources present in deeper waters, the sector has witnessed a steady shift in focus from fixed platforms to floating platforms. In the United States alone, 68% of its natural wind resources are present in deeper waters (Hartman, 2022). For such waters, use of conventional fixed foundation systems cannot be justified, calling for efficient alternatives in terms of energy output and total capital.

The Multiline Ring Anchor (MRA) (USA Patent No. US 2020/0407021 A1, 2020) is one such foundation system proposed for the floating offshore wind energy sector. This novel anchor system is developed in the geometry of a hollow cylinder (Figure 1), open at both ends with padeye(s) attached on its outer wall. The circular cross-section allows the anchor to support any type of mooring system (catenary, taut or semi-taut) without any obstruction. A key feature in the design of the MRA is the ability of the anchor to be shared multiple platforms. offshore conventional anchor systems, moored to a single turbine, the MRA can be attached to multiple turbines (Figure 2), in effect reducing the total number of anchors needed in a farm by almost 80% (Fontana, et al., 2018).

The limited consequential increase (Fontana, et al., 2018) (Pillai, et al., 2022) in the net anchor force is achievable by the MRA's design feature of supporting deep soil installations, where higher soil resistances are -mobilized. The wide range of achievable embedment depths, along with simple installation methods, and its uniform adaptability in different soil conditions, also makes the MRA an ideal choice for supporting the everincreasing scale of offshore wind turbines being installed globally.

The reduced size of the MRA compared to conventional anchor systems, along with the requirement of fewer anchors due to anchor-sharing, is expected to lower the material, capital and time for

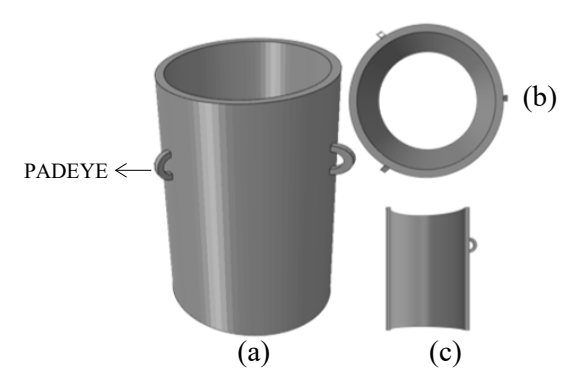


Figure 1. (a) Multiline ring anchor (MRA); (b) Top view of MRA; (c) Section cut of MRA

fabrication and installation, resulting in an increase in the efficiency of the product and ultimately, the FOWT sector.

The current paper is a part of a study aiming to serve as a proof of concept for the proposed anchor system. The paper focusses on analysing the ultimate capacity response of the MRA when subjected to monotonic, purely vertical and purely horizontal loading conditions. Congruous with earlier studies on anchor responses (Andersen, Jostad, & Dyvik, 2008) (Houlsby, Kelly, & Byrne, 2005), the resistance mechanism in the case of the application of a purely vertical load, is produced by the friction interaction between the side of the anchor and the soil, and the end bearing response at the tip of the anchor, as demonstrated in Figure 3.

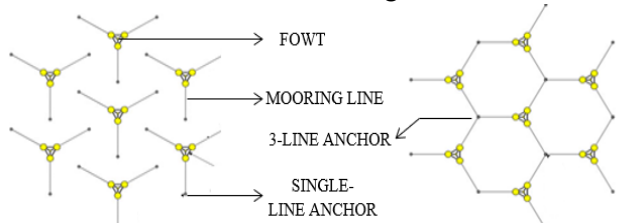


Figure 2. Layout of single line and multiline anchor system (Fontana, et al., 2018)

#### 2 NUMERICAL MODEL

A three-dimensional finite element analysis was employed to assess the behavior of a multiline ring anchor in dense sand soil conditions. The primary focus of the study was to provide estimates of ultimate load capacities of the anchor under axial and lateral loading conditions. To simulate the needed response, the model was subjected to a monotonic test load representing the resultant load on the MRA from the multiple mooring lines. For the pure vertical translation, the model location of the pad-eye for the application of the load was set at the top of the anchor's vertical axis of symmetry, whereas for the pure horizontal condition, it was set on the outer wall of the anchor at the optimal load attachment depth (Figure 4).

The FE analysis was performed using the numerical formulation available in the commercial software package ABAQUS/Standard. A fully coupled model was developed, with the effective stress principle adopted to predict its behavior and limiting the generation of excess pore pressure to model a fully drained condition. The soil domain was consequently meshed using continuum displacement and pore pressure elements (C3D6P and C3D8RP) from the ABAQUS element library. The structure of the MRA was modelled as a rigid, wished-in-place foundation system in the isotropic soil medium The mesh was graded radially and vertically to ensure computational efficiency, with increasing order of fineness closer to the structure defined using a geometric progression series, with the minimum width of an element limited to 0.1m. An element size check was also included in the mesh

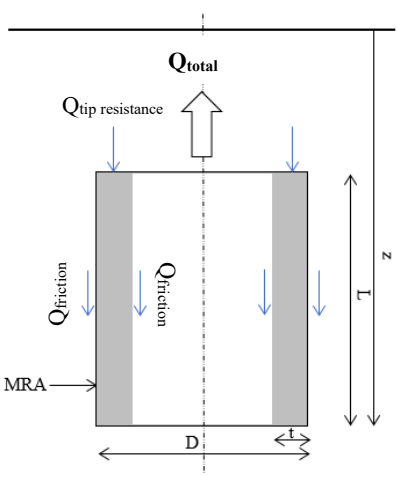


Figure 3. Resistance mechanism of the MRA under a pure vertical uplift.

generator, restricting the ratio of length to width of any side of an element to less than 8 to avoid numerical singularity concerns. The domain size has been sufficiently set radially at 3.5 times the diameter and vertically at 2.5 times the embedment depth of the anchor to annul any boundary condition effects during the loading simulations. Movement was restrained radially and vertically at the bottom and the far field of the soil domain. A sketch of the FE mesh generated is presented in Figure 5; the MRA is demonstrated as a ring of diameter D, wall thickness t, length L and embedment depth, z.

The monotonic test loads were applied using a displacement control analysis. The anchors were subjected to uniform displacement until a target displacement of 10% of the anchor diameter was achieved in the loading direction. In the case of the pure vertical loading, the action of the narrow annular area of the MRA pushing against the dense soil body gave rise to numerical convergence errors due to the formation of a region of very high stress concentration. In an effort to overcome this issue, the elements surrounding the tip of the MRA were remodelled to demonstrate a linearly elastic behaviour (Cerfontaine, Collin, & Charlie, 2016) with reduced strength. An initial estimation of the stress reduction factor for this was attained by back calculating the effective vertical stress of the soil at the top tip of the

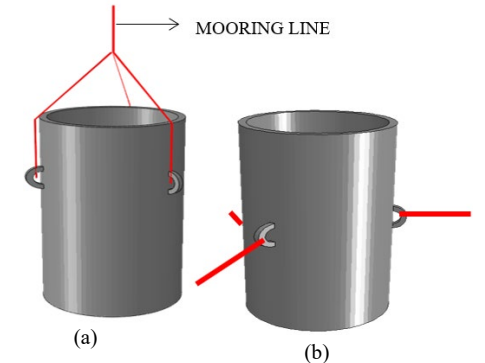
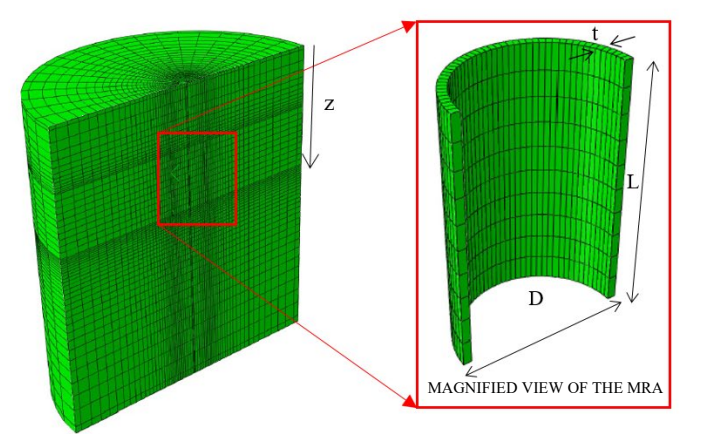


Figure 4. MRA loading conditions studied (a) Pure vertical loading; (b) Pure horizontal loading



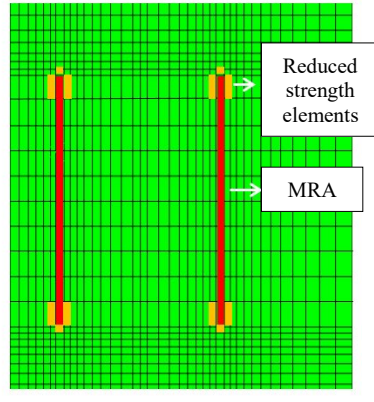


Figure 5. (a) 3D FE mesh of the MRA in cross-sectional cut view; (b) Cross-sectional cut of the mesh highlighting the reduced strength elements

MRA and comparing against the estimated soil profile. The factor was furthered refined during calibration of the FE model against the scale Centrifuge tests, as detailed in subsequent sections and set at 0.05. This region was restricted to a single element adjacent to the bottom and top tips of the anchor, and the first and last elements in the first column of elements adjacent to the inner and outer walls of the anchor. The selected elements have been identified in Figure 5b. The other soil-anchor interacting surfaces were modelled using the ABAQUS in-built isotropic Coulomb friction model.

# 2.1 Material parameters

The study focused on Ottawa F-65 sand at a relative density of 80%, categorized as medium-high density. The sand was analysed at a fully drained condition, with a saturated unit weight of 20.18 kN/m3. A Poisson's ratio, v, of 0.3, and a coefficient of earth pressure at rest dependent on the critical state friction angle (1-sin  $\varphi_{crit}$ ) were adopted. The soil behavior was modelled using the elastoplastic Mohr Coulomb constitutive model, with a non-associative flow rule. The non-associative flow rule aids in improving the plasticity predictions by Mohr Coulomb. A stress dependent Young's Modulus, E is defined in terms of a rigidity index as shown by Eq. 1 (Vesic, 1972):

$$E = I_r(2(1+v)(\sigma_v' tan\varphi_{max}))$$
 (1)

In this formulation E is a function of a density and stress-level dependent rigidity index,  $I_r$ , as proposed by Al Hakeem and Aubeny (Al Hakeem & Aubeny, 2019).

$$I_r = (aI_D + b)[m_o + m_1 \log(\sigma'_c) + m_2 \log^2(\sigma'_c)]$$
 (2)

The variables  $(a, b, m_0, m_1 \text{ and } m_2)$  in the equation are detailed in (Al Hakeem & Aubeny, 2019) based on the relative density,  $I_D$ , and confining stress,  $\sigma'_c$ .

The strength parameters of the constitutive model, the angle of internal friction and the corresponding dilation angle were defined using the equations proposed by Bolton (Bolton, 1986). This permits the generation of a soil profile with varying friction and dilation angles as functions of the mean effective stress and the relative density of the soil.

$$0.8\psi_{max} = 3I_R = \varphi_{max} - \varphi_{crit} \tag{3}$$

$$I_R = I_D (10 - \ln \sigma_{mean}') - 1 \tag{4}$$

where  $\varphi_{max}$  is the peak friction angle,  $\varphi_{crit}$  is the critical state angle,  $\psi_{max}$  is the dilation angle,  $I_R$  is the relative dilatancy index, defined using the relative density of the soil,  $I_D$  and mean effective stress,  $\sigma_{mean}'$ . The critical state friction angle for the soil is equal to 30° (Bastidas, 2016). An example set of the model parameters calculated at the soil depth equal to the vertical midpoint of the MRA for both the embedment depths are presented in Table 1.

The MRA was modelled as a steel structure with a Young's Modulus of 70 GPa, and Poisson's ratio of 0.3.

Table 1 Mohr Coulomb parameters at the midpoint depth of the MRA for the two embedment depths

	z/D = 3	z/D = 6
Young's Modulus, E (kPa)	15202.17	26735.67
Peak friction angle, $\varphi_{max}$	$40^{\rm o}$	38°
Peak dilation angle, $\psi_{max}$	13 °	11°
Poisson's ratio, v	0.3	0.3

# 3 RESULTS

3

### 3.1 Reference case results

As the first step to determine the ultimate capacity of the MRA in sand, a reference FE anchor system was modelled with a diameter, D of 2.8 m, wall thickness, t of D/20, length, L of 1.5D and embedded at a depth of 3D (termed as shallow) and 6D (termed as deep). Trends in anchor behavior when subjected to the testing conditions were studied in detail using this reference system. This case was further adopted in the calibration process of the FE model with the reduced scale centrifuge test data. The ultimate load capacities are

expressed in terms of bearing factors to normalize the model outputs. The bearing factors are defined as functions of the effective stress of the soil, and the cross-sectional area in the direction of the applied load.

The lateral bearing factor, N<sub>h</sub> is expressed as:

$$N_h = \frac{H}{\sigma_{v'}LD} \tag{5}$$

where, H is the ultimate lateral capacity as predicted by the FE model and  $\sigma_{v}'$  is the effective vertical stress. The vertical bearing factor,  $N_{v}$  is expressed as:

$$N_{v} = \frac{Q_{tv} - Q_{fv}}{\sigma_{v}' A_{tip}} \tag{6}$$

where,  $Q_{tv}$  and  $Q_{fv}$  are the ultimate vertical capacity and the vertical capacity due to skin friction, respectively,  $\sigma_{v}'$  is the effective vertical stress at the tip of the anchor, and  $A_{tip}$  is the annular area of the anchor. The results in terms of their bearing capacity factors are presented in Table 2. The factors in the table represent the end points of the capacity yield curve for each depth to diameter ratio (Zhao, et al., 2019). For the vertical loading conditions, the capacity predicted by the model is 3.07 MN, and 13.69 MN for the shallow and the deeper embedment depths respectively. Out of this, 0.43 MN is produced by the frictional resistance between the anchor wall and the surrounding soil, and 2.56 MN by the tip resistance from the upper annular area of the anchor, for the shallow embedment depth. For the deeper embedment depth, the corresponding capacity contributions are 0.97 MN and 12.72 MN, respectively. This demonstration of the increase in the contribution (86% to 92.9%) of the tip resistance to the ultimate capacity with the increase in embedment depth aligns with the increase in the weight of the soil body required by the anchor to vertically push through under the tensile loading condition. For the fictional behavior between the anchor walls and the surrounding soils, the model allows for sliding to occur both at the inner and outer wall soil interfaces, as described in the earlier

Table 2 Horizontal and vertical bearing factors for different depth to diameter ratio

	Horizontal bearing factor, N <sub>H</sub>	Vertical bearing factor, N <sub>V</sub>
z/D=3	21.61	51.78
z/D = 6	23.10	89.52

section of the paper. The displacement contours in Figure 6 displays the creation of a partial soil plug inside the anchor as the vertical load is being applied. For the shallow embedment depth, the behavior results in a surface failure condition.

The horizontal loading condition is modelled to simulate a pure lateral shift of the anchor to a displacement target of 0.1D. The capacity predicted by the model for the shallow embedment depth is 10.88 MN and for the deeper embedment depth is 23.1 MN. Load attachment depth at the optimal attachment depth gives the maximum lateral capacity which for a conventional caisson anchor depth is approximately at 0.67L, however, the optimal attachment depth for MRA is somewhere around middle of the anchor (0.5L) (Aldawwas, 2022). Thus, a load attachment depth at the middle of MRA length was used.

The positive relationship observed between the embedment depth and ultimate capacity of the MRA, along with easy installation methods, provide a feasible solution to meet the load demands of bigger wind turbines.

#### 3.2 FE model validation

Centrifuge tests at the Center for Geotechnical Modeling (CGM) at the University of California at Davis were performed in collaboration with the current numerical study and was adopted as a calibrating tool for the latter. The centrifuge tests were performed in the 9 m-radius centrifuge at an acceleration of 70g. The sand soil samples were prepared by dry pluviation and significant efforts were made to maintain similar testing conditions between the numerical study and the physical tests to perform a fair comparative study. However, one important difference is that the MRA were quasi-

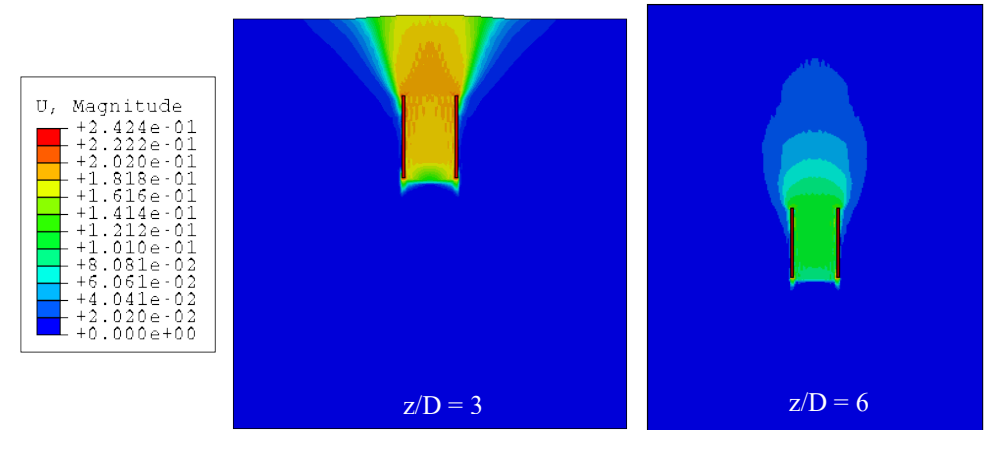


Figure 6. Displacement contours of the MRA system under a purely vertical loading condition.

statically pushed into the soil at 1g, while they were wished in place in the numerical model.

The data from the centrifuge tests were taken as representative of the testing conditions simulated in the numerical model. For the pure vertical loading conditions, the test anchor was subjected to a uniform uplift. For the lateral loading conditions, the test anchor was pulled at an angle of 30° to the horizontal, due to sizing limitations of the container to achieve the desired embedment depth for the anchor. A slightly higher capacity prediction can be expected by the FE model due to this assumption, attributed to the minor difference in purely horizontal anchor capacities vs anchor capacities at small inclination angles as observed in Zhao, et. al (Zhao, et al., 2019).

For the vertical loading conditions, the centrifuge test produced ultimate capacities of 3.11 MN for the anchor embedded to the shallow depth and 5.48 MN for the anchor at the deep embedment depth. The ultimate capacities for the physical tests reflected the peak capacities. They resulted in error percentages of 1.08% and 192.13%, respectively for the predictions made by the numerical model. A possible explanation for the high error percentage for the deeper embedment depth, unlike the shallow embedment depth, can be attributed to significant soil disturbance induced during the installation process of the anchor for the centrifuge testing. To verify this, Cone Penetration Tests (CPT) were performed in the centrifuge at a location where an anchor had been previously installed. The CPT tip resistance indicated a reduction in the relative density of the soil from 80% to 20%. This drastic fall in the relative density of the soil directly above the anchor was incorporated in the numerical model by remodeling the affected region to a relative density of 20%. The remodelling was limited to a column of soil above the anchor. The modified FE model with the disturbed soil

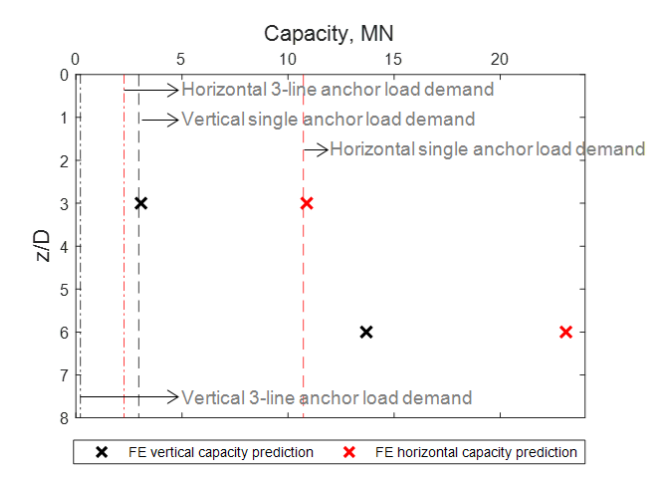


Figure 7: FE capacity predictions for different embedment (z) to diameter (D) ratio, vs. horizontal (red) and vertical (black) anchor load demand from a 15 MW turbine (Pillai, et al., 2022) with a single line mooring (short mooring radius) and a 3-line mooring (larger mooring radius) system.

produced an ultimate capacity of 5.77 MN, which brought down the error percentage to 5.4 %, well within a tolerable allowance.

For the horizontal loading conditions, the centrifuge tests provided ultimate capacities of 8.74 MN and 22.97 MN for the shallow and deep embedment depths, respectively, resulting in error percentages of 24.4% and 0.44% for the corresponding predictions by the FE model. The overestimation of the FE model can be attributed to the inclination of the load applied for the physical test, instead of a pure lateral condition.

The error percentages of the FE model predictions against the centrifuge data were considered satisfactory. The model will be further applied to study the behavior of the MRA under different loading combinations to justify its use as an efficient foundation system for floating offshore wind turbines.

# 3.3 Analysis of anchor load demand of a 15MW turbine

Figure 7 presents the capacities predicted by the FE model against the anchor load demand from a 15 MW turbine as derived by Pillai et al (Pillai, et al., 2022), as part of a single line and a 3-line anchor system. Considering the rapid growth of the size of offshore floating wind turbines used in practice, and the successful installation of a prototype 15 MW turbine by Vestas (Radowitz, 2022), it is imperative that anchors are designed to meet the demands of such turbines.

The study by Pillai et al (Pillai, et al., 2022) was based on the environmental conditions observed in the Celtic Sea off the coast of UK. The 15 MW IEA turbine was supported on a semi-submersible platform, and analyzed under severe operating sea state and extreme sea state design load conditions. For the case of the single line system, the peak anchor loads, observed for the shortest mooring radius were satisfied by the deeply embedded MRA. The vertical load demand of 2.96 MN, as well as the horizontal load demand of 10.72 MN were well within the capacities predicted by the FE model for the deeply embedded MRA.

For the 3-line anchor sharing case, the analysis was carried out for a larger mooring radius to ensure adequate space between the anchors. The system observed a reduction in the horizontal anchor load compared to the single line anchor under an identical mooring radius, due to the placement of the padeyes (and the mooring lines) on the MRA wall in balancing opposing directions but a two-fold increase in the vertical anchor load. Despite the increase in the vertical load demand for the studied mooring radius, it was met by the vertical capacities predicted for the shallow, as well as the deeply embedded MRA model. This, along with the response of the horizontal loading condition, is presented in Figure 7. Additional capacity can still be attained by increasing the embedment depth of the

anchor. This exercise, thus, successfully demonstrates the ability of the MRA to meet the needs of a rapidly developing sector.

### 4 CONCLUSIONS

This paper presents a part of a study on a novel anchor system, the Multiline Ring Anchor (MRA), proposed to support floating offshore wind turbines. A numerical analysis was conducted on the behaviour of the MRA under monotonic loading conditions, using a 3D finite element model, to predict estimates of axial and lateral ultimate capacities. The FE model was further calibrated against data from a reduced scale centrifuge test performed under comparative conditions. The study concluded the following:

- Lateral capacity of 10.88 MN for a shallow embedment depth, and 23.08 MN for a deep embedment depth were predicted by the FE model for the reference case.
- Axial capacity of 3.07 MN for a shallow embedment depth, and 13.69 MN for a deep embedment depth were predicted by the FE model for the reference case
- Calibration against centrifuge test data resulted in error percentages of 24% and 0.44% for the lateral capacities at shallow and deep embedment depths.
- For the vertical tests for the deep embedment depth in the centrifuge, significant soil disturbance was induced in the centrifuge tests, which had to be incorporated in the FE model. With the modified FE model, the error percentage between numerical model and the centrifuge was 5.4 %.

The capacities of the MRA as predicted by the numerical model also satisfied both the axial and the lateral anchor load demands of a 15 MW turbine as studied by Pillai et al (Pillai, et al., 2022), further strengthening the justification to adopt the MRA as an anchor system for floating offshore wind turbine.

#### 5 ACKNOWLEDGEMENTS

The authors would like to acknowledge the support from National Science Foundation, award number CMMI-1936901 and the Texas A&M High Performance Research Computing facility for the use of their resources in running the numerous finite element analyses supporting this study.

### 6 REFERENCES

Al Hakeem, N., & Aubeny, C. P. (2019). Numerical Investigation of Uplift Behavior of Circular Plate Anchors in Uniform Sand. *Journal of Geotechnical and Geoenvironmental Engineering*.

- Aldawwas, A. S. (2022). *Ultimate Load Capacity of Caisson Foundations and Anchors in Sand*. Doctoral dissertation, Texas A&M University.
- Andersen, K. H., Jostad, H. P., & Dyvik, R. (January 2008). Penetration Resistance of Offshore Skirted Foundations and Anchors in Dense Sand. *Journal of Geotechnical and Geoenvironmental Engineering*.
- Aubeny, C. P., Diaz, B. D., Arwade, S. R., DeGroot, D. J., Landon, M. E., Fontana, C., & Hollowell, S. T. (2020). USA Einkaleyfi nr. US 2020/0407021 A1.
- Bastidas, A. M. (2016). *Ottawa F-65 Sand Characterization*. Davis: University of California.
- Bolton, M. (1986). The shear strength and dilatancy of sands. *Geotechnique*, 65-78.
- Cerfontaine, B., Collin, F., & Charlie, R. (2016). Numerical modelling of transient cyclic vertical loading of suction caissons in sand. *Géotechnique*, 121-136.
- Fontana, C. M., Hallowell, S. T., Arwade, S. R., DeGroot, D. J., Landon, M. E., Aubeny, C. P., . . . Ozmutlu, S. (2018). Multiline anchor force dynamics in floating offshore wind turbines. *Wind Energy*, 1177-1190.
- Hartman, L. (16. August 2022). Energy Efficiency and Renewable Energy. Sótt frá https://www.energy.gov/eere/wind/articles/top-10-things-you-didnt-know-about-offshore-wind-energy
- Houlsby, G. T., Kelly, R., & Byrne, B. W. (2005). The Tensile Capacity of Suction Caissons in Sand under Rapid Loading. *Proceedings of the International symposium on frontiers in offshore geotechnics*, 405-410.
- Pillai, A., Gordelier, T., Thies, P., Dormenval, C., Wray, B., Parkinson, R., & Johanning, L. (2022). Anchor loads for shallow water mooring of a 15 MW floating wind turbine Part I: Chain catenary moorings for single and shared anchor scenarios. Ocean Engineering.
- Radowitz, B. (December 2022). 'Great step forward'.

  Sótt frá Recharge:
  https://www.rechargenews.com/wind/great-stepforward-vestas-15mw-offshore-wind-giantproduces-first-power/
- Vesic, A. S. (1972). Expansion of cavities in infinite soil mass. *Journal of Soil Mechanics & Foundations Div*, 265-290.
- Zhao, L., Gaudin, C., O'Loughlin, C. D., Hambleton, J. P., Cassidy, M. J., & Herduin, M. (2019). Drained Capacity of a Suction Caisson in Sand unde Inclined Loading. *Journal of Geotechnical and Geoenvironmental Engineering*.